Journal of Alloys and Compounds 490 (2010) 98–102

Contents lists available at ScienceDirect

Journal of Alloys and Compounds

journal homepage: www.elsevier.com/locate/jallcom

Solution chemistry synthesis, morphology studies, and optical properties of five distinct nanocrystalline Au–Zn intermetallic compounds

Zachary L. Schaefer, Dimitri D. Vaughn II, Raymond E. Schaak*

Department of Chemistry and Materials Research Institute, The Pennsylvania State University, University Park, PA 16802, United States

ARTICLE INFO

Article history:
Received 21 July 2009
Received in revised form 8 October 2009
Accepted 17 October 2009
Available online 27 October 2009

Keywords:
Nanostructured materials
Intermetallics
Chemical synthesis

ABSTRACT

Au–Zn was used as a prototype binary system for exploring intermetallic phase accessibility in nanoparticle systems using low-temperature solution chemistry methods. By reacting Au nanoparticles with diethylzinc (Et_2Zn) in oleylamine at temperatures of 250–300 °C, nanoparticles of five distinct binary intermetallic compounds were accessible: Au_3Zn, Au_5Zn_3, AuZn, Cu_5Zn_8-type γ-(Au,Zn), and Mg-type ε-(Au,Zn). A variety of nanoparticle shapes, including spheres, triangles, hexagons, and rods, are accessible in the Au–Zn system via a pseudomorphic reaction of Au nanocrystal shapes with Et_2Zn. The Au–Zn nanoparticles have optical properties that vary with Zn content, ranging from a surface plasmon resonance peak at ~495 nm for Au_3Zn to absorption in the ultraviolet region for the Zn-rich phases.

1. Introduction

While intermetallic compounds of the late transition metals are typically synthesized using high-temperature metallurgical techniques, alternative low-temperature methods have opened the door to new phases [1–13], high-quality single crystals [5,7,9,11,12], thin films [2,14,15], and materials with a variety of nano- and micro-structures [16–18] that the traditional methods generally cannot access. Among these, low-temperature solution chemistry techniques have emerged as a useful platform for synthesizing intermetallic compounds as nanocrystals, often with the capability of controlling particle shape and size [19–27] and sometimes providing access to non-equilibrium phases [10,13,28]. Despite these benefits, one of the key challenges inherent in using solution chemistry techniques to synthesize intermetallics is the ability to access multiple stable phases in a binary system. One phase tends to form first, and while in some cases it may be possible to access other phases directly after appropriate system-dependent optimization, it is often necessary to use multi-step reactions to generate other stable phases [29]. To date, there have been no extensive studies on a single binary intermetallic system with the goal of defining the parameters that allow multiple phases to form as nanocrystals using solution chemistry synthesis techniques.

Au–Zn is an excellent prototype system for studying phase accessibility using solution chemistry methods. The Au–Zn phase diagram has been studied extensively, both computationally [30] and experimentally [31–37], and a large number of phases exist. The structural and compositional diversity of this binary system, coupled with the useful properties of some of the phases, make it a prudent system to study from a solution chemistry perspective. For example, AuZn is a prototype shape memory alloy [38–40], and nanostructured AuZn could serve as a model system for low-temperature nanoscale actuation. Au_3Zn has also been reported to undergo a martensitic transformation [41]. The surface plasmon resonance of Au is known to vary by alloying and incorporating zinc [21], which could allow composition-induced tuning of color in Au–Zn alloy nanoparticles [42–44]. The Au–Zn system is also important in the development of new low-melting solders to replace lead based solders for electronic packaging applications [45–47].

In this paper, we explore intermetallic phase formation in the Au–Zn system using solution-based nanocrystal synthesis techniques. Using high-boiling long-chain amine solvents (e.g. oleylamine), as well as the Au and Zn reagents chloroauric acid ($HAuCl_4$) and diethylzinc (Et_2Zn), respectively, we are able to synthesize nanoparticles of five distinct Au–Zn intermetallic compounds, which represents the largest number of phases reported to date that have been accessible in a single binary system using solution chemistry methods. The accessible intermetallics, targeted to span a range of Au–Zn compositions and not intended to be exhaustive, are Au_3Zn, Au_5Zn_3, AuZn, Cu_5Zn_8-type γ-(Au,Zn), and Mg-type ε-(Au,Zn). All of these phases are accessible as stable colloidal dispersions of largely spherical particles, most with diam-

* Corresponding author at: Department of Chemistry and Materials Research Institute, 104 Chemistry Building, The Pennsylvania State University, University Park, PA 16802, United States. Tel.: +1 814 865 8600; fax: +1 814 863 8403.
E-mail address: schaak@chem.psu.edu (R.E. Schaak).

0925-8388/$ – see front matter © 2009 Elsevier B.V. All rights reserved.
doi:10.1016/j.jallcom.2009.10.137

Table 1
Detailed synthesis parameters for Au–Zn phases.

	Au_3Zn	Au_5Zn_3	AuZn	γ-(Au,Zn)	ε-(Au,Zn)
$HAuCl_4{\cdot}xH_2O$ (mmol)	0.05	0.05	0.05	0.05	0.05
Et_2Zn (mmol)	0.15	0.20–0.25	0.25–0.30	0.30–0.40	0.50
Zn:Au ratio	3:1	4–5:1	5–6:1	6–8:1	10:1
Temperature (°C)	250–280	250–280	300–320	280–300	280–300
Time (min)	30	30	30	30	30

eters of 10–30 nm. Consistent with their compositional variation, the Au–Zn nanoparticles exhibit surface plasmon bands ranging from 495 nm to ultraviolet wavelengths.

2. Experimental

2.1. Materials

All solvents were de-gassed by freeze–thaw-pump cycles and chemicals were used as received and stored in a dry box under Ar. The following solvents were used: $CH_3(CH_2)_7CHCH(CH_2)_8NH_2$ [oleylamine, TCI America, min. 40.0%] and $(C_6H_5)_2O$ [diphenyl ether, Sigma–Aldrich, 98%]. The following metal reagents used were: $HAuCl_4{\cdot}xH_2O$ [chloroauric acid, Sigma–Aldrich, 99.9%] and $Zn(C_2H_5)_2$ [diethylzinc, Et_2Zn, Sigma–Aldrich, 1 M solution in hexane].

2.2. Synthesis

Each intermetallic product was made using a one-pot reaction in which metal precursors were thermally decomposed in hot organoamine solvent. All metal precursors were prepared in an Ar-filled drybox using small scintillation vials, while the reactions were carried out in a 3-neck round bottom flask fitted with a condenser, thermometer adapter, thermometer, and rubber septum. All reactions were carried out under an Ar atmosphere using standard Schlenk techniques. First, Au nanoparticles were made in situ by dissolving $HAuCl_4{\cdot}xH_2O$ (20 mg, 0.05 mmol) in oleylamine (2 mL) by sonication for 10 min (forming an orange-colored solution), followed by injection of the Au solution into hot oleylamine (5 mL) at ~220 °C (forming a wine-red colored solution). This solution was then allowed to age until the necessary temperature for Et_2Zn injection was reached (typically 5–10 min, see Table 1 for temperatures). Once this temperature was reached, a 1-mL Et_2Zn–oleylamine solution was added drop wise to the Au nanoparticle solution, causing an immediate color change to form a black/purple solution. The reaction was allowed to heat for approximately 30 min and then slowly cooled by removing the flask from the heating mantle. Specific details for synthesizing each intermetallic product are included in Table 1. The nanoparticle shapes shown in Fig. 4 were made in a similar manner to that described above, except that $HAuCl_4{\cdot}xH_2O$ was dissolved in diphenyl ether (2 mL) containing oleylamine (0.0167 mL, 0.05 mmol) and diphenyl ether (5 mL) was substituted as the solvent.

2.3. Characterization

Powder X-ray diffraction (XRD) data were collected on a Bruker Advance D8 X-ray diffractometer using Cu Kα radiation. Transmission electron microscopy (TEM) images and selected area electron diffraction (SAED) patterns were collected using a JEOL JEM 1200 EXII microscope operating at 80 kV. Samples for TEM analysis were prepared by sonication of the nanoparticles in toluene or hexanes and drop coating onto the surface of a carbon coated copper grid. Scanning electron microscopy (SEM) and energy dispersive X-ray spectroscopy (EDS) data were collected using a JEOL JSM 5400 scanning electron microscope. UV–Visible spectroscopy data were collected on nanoparticle samples dispersed in toluene using an Ocean Optics DH-2000-BAL spectrometer with quartz cuvettes.

3. Results and discussion

The synthetic process, described previously for PdZn, Cu_5Zn_8, Au_3Zn, and highly impure AuZn [21], involves the reaction of Au nanoparticles, formed either in situ or ex situ, with Et_2Zn at elevated temperatures in a high-boiling organoamine solvent. This is an example of "conversion chemistry," where pre-formed nanoparticles can serve as a template for chemical transformation into a derivative phase, often with retention of key morphological features [24]. In this case, Au nanoparticles react with the Zn that is liberated following the decomposition of Et_2Zn, forming Au–Zn intermetallics upon diffusion of Zn into the Au particles. In our investigations of the Au–Zn system, Au nanoparticles were formed in situ, followed by the addition of different amounts of Et_2Zn to access five distinct intermetallic phases (Table 1). Powder XRD patterns for the accessible Au–Zn intermetallics – Au_3Zn, Au_5Zn_3, AuZn, γ-(Au,Zn), and ε-(Au,Zn) – are shown in Fig. 1. The experimental data agree well with the simulated data, confirming the

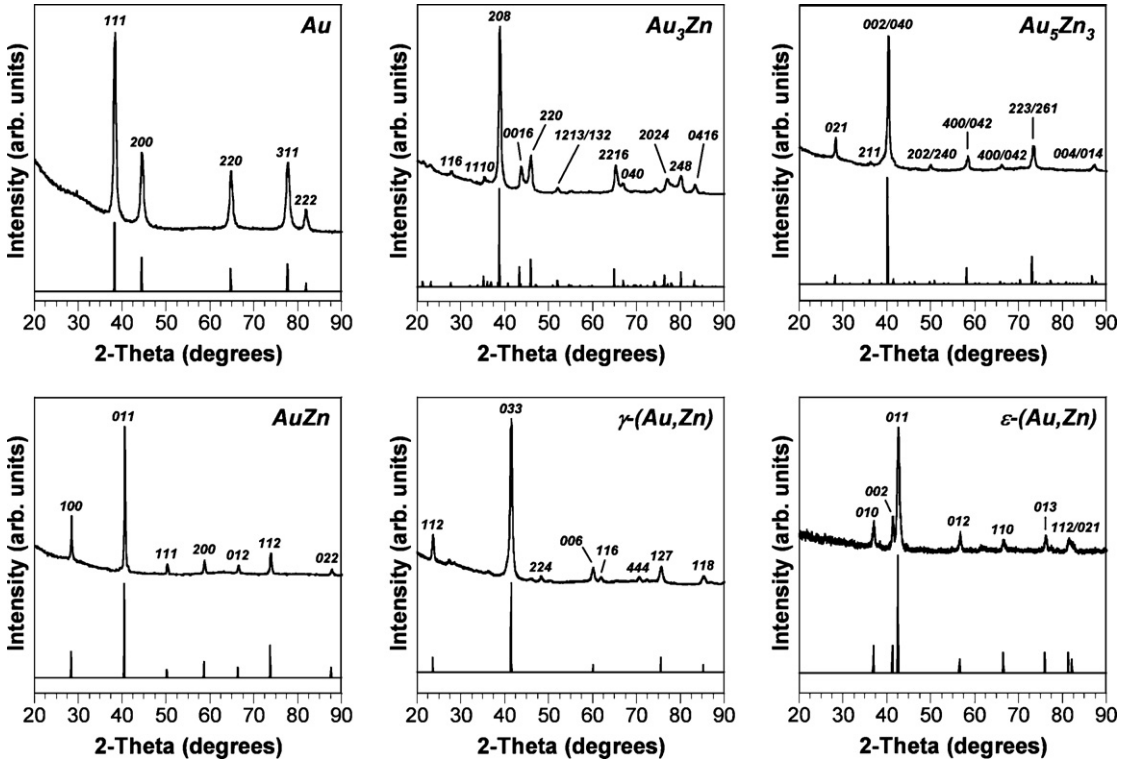

Fig. 1. Powder XRD patterns of Au, Au_3Zn, Au_5Zn_3, AuZn, γ-(Au,Zn), and ε-(Au,Zn). Simulated patterns are shown below the experimental data and are based on data in Pearson's Handbook. The simulated pattern for γ-(Au,Zn) is based on the crystal structure of Pd_2Zn_9, as described in the text.

phase identification. Au_3Zn, Au_5Zn_3, and AuZn match patterns 65-1630, 65-9647, and 65-5430, respectively, in the PDF-2 database, 2006 edition, and the simulated XRD patterns are based on the crystal data in Pearson's Handbook. The XRD patterns for AuZn and Au_5Zn_3 appear similar, but based on the prior literature reports [31,33,48] and comparison with the simulated data, both are distinct phases that are each accessible using this solution chemistry technique. The XRD pattern for ε-(Au,Zn) matches that of $Au_{1.2}Zn_{8.8}$ (65-8027) in the PDF-2 database, and the simulated XRD pattern is based on a standard hcp lattice (Mg structure type). Cu_5Zn_8-type γ-(Au,Zn) has a small (≤5%) AuZn impurity and ε-(Au,Zn) shows some crystalline ZnO (5–10%), but the others appear phase pure within the detection limits of our laboratory powder XRD.

Cu_5Zn_8-type γ-(Au,Zn) appears on the Au–Zn phase diagram with a wide composition window that ranges from 62.5% to ~76% Zn, and its formation and stability have been questioned in the literature [36]. To confirm the formation of this phase, we performed a full-pattern decomposition using the Le Bail method [49] since crystal data and experimental powder XRD patterns were not found in either Pearson's Handbook or the PDF-2 2006 database. The powder XRD pattern for γ-(Au,Zn) matched well with that of Cu_5Zn_8-type Pd_2Zn_9, which has been extensively characterized [50] and serves as an effective structural model. The results of the full-pattern decomposition using the Le Bail method, based on the space group for Pd_2Zn_9 ($I\bar{4}3m$, #217) and the experimentally determined lattice constant for our sample of γ-(Au,Zn) [a = 9.2528(2) Å], are shown in Fig. 2. The Le Bail fit yielded R_{exp} = 2.36%, R_{wp} = 4.85%, and R_p = 3.57%, and included both γ-(Au,Zn) and a ~10% impurity of AuZn (marked by asterisks in Fig. 2). The lattice constant of our experimental phase compares favorably with that of the reported lattice constant for γ-(Au,Zn) (a = 9.245 Å) [34], and the Le Bail fit accounted for every observed reflection. It is worth noting that over time at room temperature, the nanoparticles of γ-(Au,Zn) begin to decompose to AuZn and Zn (evident as ZnO by XRD because of the unavoidable oxidation of nanocrystalline Zn).

Fig. 3 shows TEM images and SAED patterns for the Au–Zn nanoparticles, as well as the Au templates. The as-made Au nanoparticle samples are generally polydisperse spheres, with some faceting present. (The focus of this study is on phase accessibility, not on synthesizing monodisperse nanoparticles. The polydisperse Au nanoparticle templates are sufficient for this purpose, and particle size and dispersity can be improved as needed, as shown previously [21].) The Au_3Zn, AuZn, and Au_5Zn_3 particles have similar morphologies, sizes, and size distributions, and are similar in these characteristics to the Au nanoparticles used as templates. The SAED patterns corresponding to the TEM images match the XRD patterns for the bulk samples, and thus confirm the phase identification. Representative TEM images of the ε-(Au,Zn) and γ-(Au,Zn) particles are shown in Figs. 3e and 2, respectively. These Zn-rich particles tend to be larger, more polydisperse, and faceted with a greater proportion of cube-shaped morphologies than the Au-rich and equiatomic phases, indicating additional particle growth and coalescence as more zinc is added.

With the exception of the Zn-rich phases, the morphologies of the Au–Zn products closely match those of the Au particle templates. This pseudomorphic relationship implies that other Au–Zn shapes could be accessible if appropriate Au templates are avail-

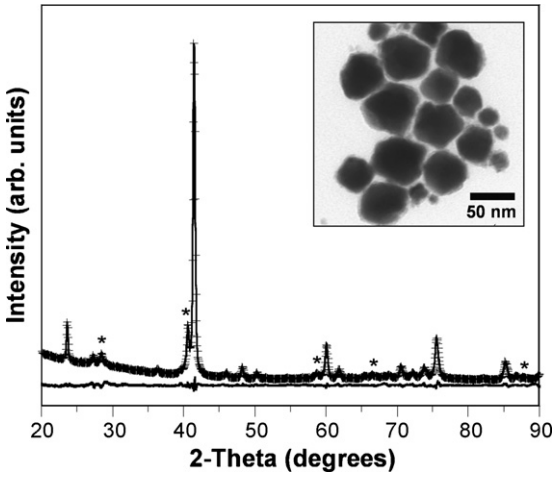

Fig. 2. Le Bail fit of the powder XRD data for γ-(Au,Zn) [space group $I\bar{4}3m$, a = 9.2528(2) Å], showing the experimental data (crosses), calculated pattern (solid line), and difference curve (bottom). AuZn impurity peaks are indicated by asterisks. The inset shows a representative TEM image of the γ-(Au,Zn) nanoparticles.

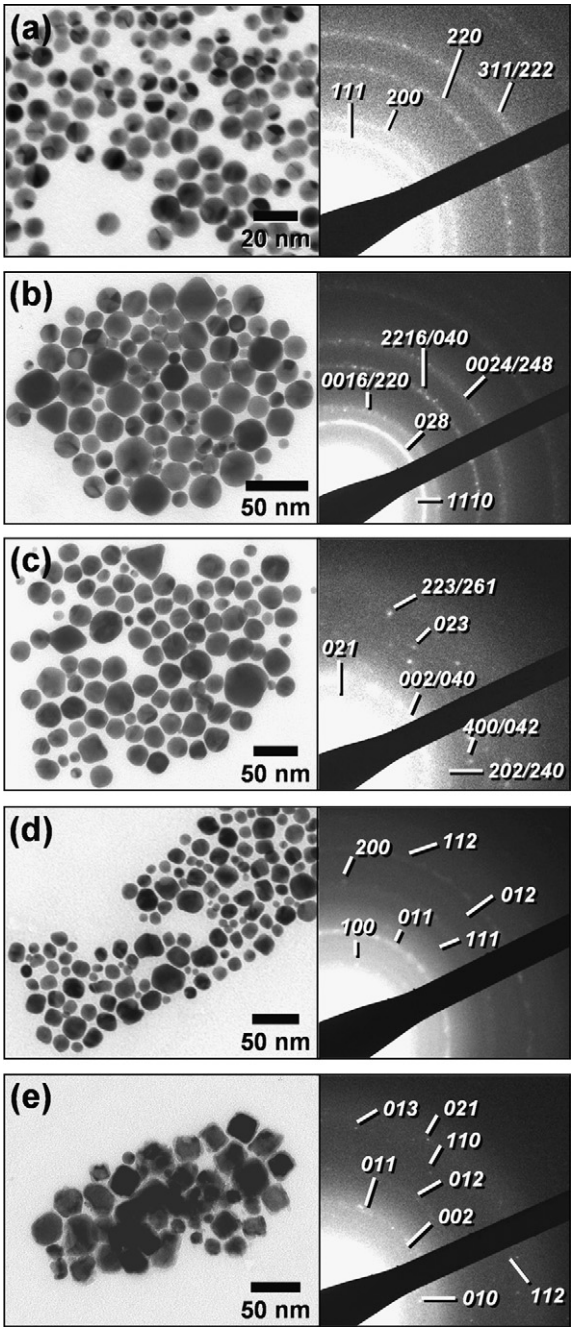

Fig. 3. Representative TEM images and SAED patterns for nanoparticles of (a) Au, (b) Au_3Zn, (c) Au_5Zn_3, (d) AuZn, and (e) ε-(Au,Zn).

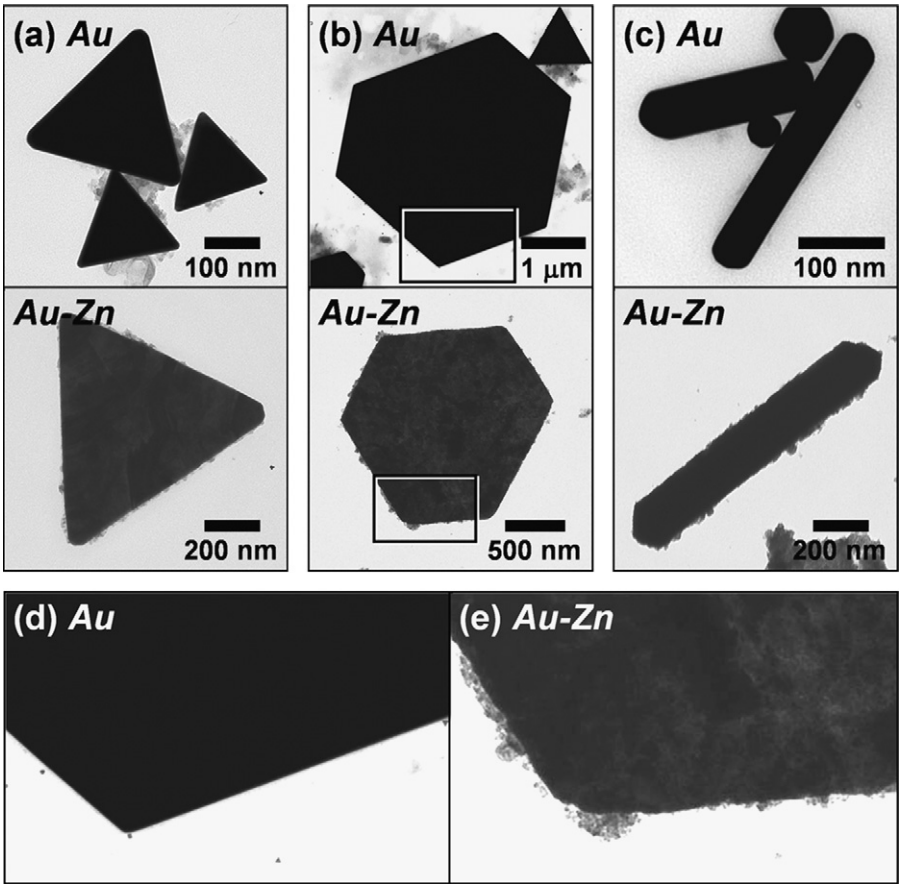

Fig. 4. TEM images of nanocrystal (a) triangles, (b) hexagons, and (c) rods of Au (top) and AuZn (bottom, after reaction of the Au nanocrystal shapes with Et_2Zn). Panels (d) and (e) highlight the change in nanostructure upon reaction of Au nanocrystal shapes (d) with Et_2Zn (e).

able. Fig. 4 shows TEM images that include triangles, hexagonal platelets, and rods from a sample of Au nanoparticle shapes produced when 5 mL of diphenyl ether is used as the hot solvent instead of 5 mL of oleylamine. Even though the templates are quite large (750 nm to 3 μm) after reaction with Et_2Zn, the products (mostly AuZn with some Au_3Zn regions) maintain the shapes of the Au nanoparticle templates, as shown in Fig. 4. An enlarged region of one of the hexagon-shaped Au nanocrystal templates (Fig. 4d) and the hexagon-shaped Au–Zn product (Fig. 4e) shows morphological evidence of the reaction, with rougher edges and a more polycrystalline nanostructure.

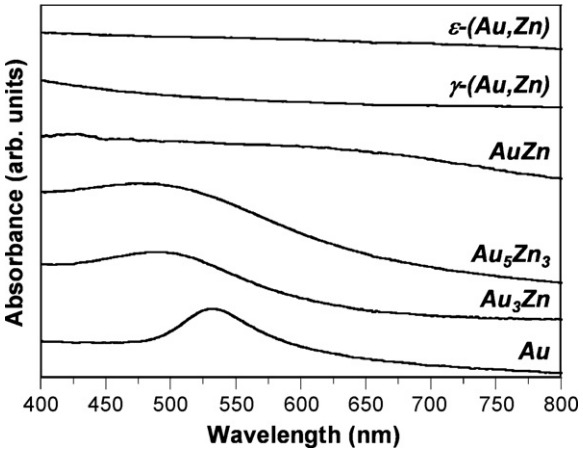

Fig. 5. UV–visible absorbance spectra (nanoparticles dispersed in toluene) for Au, Au_3Zn, Au_5Zn_3, AuZn, γ-(Au,Zn), and ε-(Au,Zn).

As a preliminary investigation of the characteristic properties of these Au–Zn nanoparticles across the range of accessible compositions, UV–Visible spectroscopy was used to determine the shift of the surface plasmon peak of Au upon incorporation of Zn. Au is well known to have a visible-wavelength surface plasmon resonance peak that is near 530–535 nm for isotropic spherical particles in toluene [51,52]. Zn has a surface plasmon resonance in the UV [53,54], so alloying Au with Zn would be expected to produce a blue shift. UV–Vis data for the Au–Zn nanoparticles in toluene are shown in Fig. 5. The Au nanoparticles absorb at 535 nm, as expected. Au_3Zn is blue shifted relative to Au, absorbing at 495 nm and consistent with what we observed previously [21]. Au_5Zn_3 is further blue shifted, with λ_{max} = 485 nm. AuZn, ε-(Au,Zn), and γ-(Au,Zn) appear black and have nearly flat UV–Vis spectra, consistent with what is expected based on the higher Zn content.

4. Conclusions

In this paper, we have expanded the capabilities of solution-based "conversion chemistry" strategies for synthesizing nanoparticles of binary intermetallic compounds. Specifically, using Au–Zn as a prototype system, we were able to access nanocrystals of five distinct Au–Zn phases – Au_3Zn, Au_5Zn_3, AuZn, Cu_5Zn_8-type γ-(Au,Zn), and Mg-type ε-(Au,Zn) – by reacting Au nanoparticles with Et_2Zn in oleylamine at 250–300 °C. This represents the largest number of distinct intermetallic compounds reported to date that can be accessed in a single binary system using low-temperature solution chemistry methods. From these studies, it appears that multiple phases can indeed be accessed in a single binary system

using solution chemistry methods by careful control of reagent stoichiometry and temperature, although additional studies with different systems will be necessary to generalize this conclusion. For the case of AuZn, shape retention appears feasible and represents the first example of nanocrystal shapes in shape memory alloy systems. While preliminary, this could open the door to interesting studies of size- and morphology-dependent mechanical properties at nanometer length scales. The Au–Zn nanoparticles have optical properties that vary with Zn content, ranging from a surface plasmon resonance peak at 495 nm for Au_3Zn to UV-absorption for the Zn-rich phases.

Acknowledgments

This work was supported by the U.S. Department of Energy (DE-FG02-08ER46483), a DuPont Young Professor Grant, a Beckman Young Investigator Award, a Sloan Research Fellowship, a Camille Dreyfus Teacher-Scholar Award, and the Penn State MRSEC (DMR-0820404). Electron microscopy was performed at the Electron Microscopy Facility at the Huck Institute for Life Sciences.

References

[1] J.H. Perepezko, Mater. Sci. Eng. 65 (1984) 125.
[2] M. Hiratani, Y. Ito, K. Miyauchi, T. Kudo, Mater. Res. Bull. 23 (1988) 1739.
[3] M. Noh, J. Thiel, D.C. Johnson, Science 270 (1995) 1181.
[4] M. Noh, C.D. Johnson, M.D. Hornbostel, J. Thiel, D.C. Johnson, Chem. Mater. 8 (1996) 1625.
[5] X.Z. Chen, P. Larson, S. Sportouch, P. Brazis, S.D. Mahanti, C.R. Kannenwurf, M.G. Kanatzidis, Chem. Mater. 11 (1999) 75.
[6] C. Suryanarayana, Prog. Mater. Sci. 46 (2001) 1.
[7] S.E. Latturner, M.G. Kanatzidis, Inorg. Chem. 43 (2004) 2.
[8] B.M. Leonard, N.S.P. Bhuvanesh, R.E. Schaak, J. Am. Chem. Soc. 127 (2005) 7326.
[9] M.G. Kanatzidis, R. Pöttgen, W. Jeitschko, Angew. Chem. Int. Ed. 44 (2005) 6996.
[10] B.M. Leonard, R.E. Schaak, J. Am. Chem. Soc. 128 (2006) 11475.
[11] E.M. Benbow, S.E. Latturner, J. Solid State Chem. 179 (2006) 3969.
[12] M. Stojanovic, S.E. Latturner, J. Solid State Chem. 180 (2007) 907.
[13] Y. Vasquez, Z. Luo, R.E. Schaak, J. Am. Chem. Soc. 130 (2008) 11866.
[14] C.H. Meyer Jr., M.F. Merriam, D.P. Snowden, J. Vac. Sci. Tech. 9 (1972) 354.
[15] K.N. Tu, G. Ottaviani, R.D. Thompson, J.W. Mayer, J. Appl. Phys. 53 (1982) 4406.
[16] Q. Guo, X. Teng, H. Yang, Adv. Mater. 16 (2004) 1337.
[17] R.E. Schaak, A.K. Sra, B.M. Leonard, R.E. Cable, J.C. Bauer, Y.-F. Han, J. Means, W. Teizer, Y. Vasquez, E.S. Funck, J. Am. Chem. Soc. 127 (2005) 3506.
[18] R.E. Cable, R.E. Schaak, Chem. Mater. 17 (2005) 6835.
[19] S. Sun, Adv. Mater. 18 (2006) 393.
[20] M. Chin, J. Kim, J.P. Liu, H. Fan, S. Sun, J. Am. Chem. Soc. 128 (2006) 7132.
[21] R.E. Cable, R.E. Schaak, Chem. Mater. 19 (2007) 4098.
[22] S. Maksimuk, S.C. Yang, Z.M. Peng, H. Yang, J. Am. Chem. Soc. 129 (2007) 8684.
[23] J.C. Bauer, X. Chen, Q. Liu, T.-H. Phan, R.E. Schaak, J. Mater. Chem. 18 (2008) 275.
[24] Y. Vasquez, A.E. Henkes, J.C. Bauer, R.E. Schaak, J. Solid State Chem. 181 (2008) 1509.
[25] H. Abe, F. Matsumoto, L.R. Alden, S.C. Warren, H.D. Abruña, F.J. DiSalvo, J. Am. Chem. Soc. 130 (2008) 5452.
[26] S.C. Yang, Z.M. Peng, H. Yang, Adv. Funct. Mater. 18 (2008) 2745.
[27] T. Ghosh, F. Matsumoto, J. McInnis, M. Weiss, H.D. Abruña, F.J. DiSalvo, J. Nanopart. Res. 11 (2009) 965.
[28] K. Senevirathne, R. Tackett, P.R. Kharel, G. Lawes, K. Somaskandan, S.L. Brock, ACS Nano. 3 (2009) 1129.
[29] R.E. Cable, R.E. Schaak, J. Am. Chem. Soc. 128 (2006) 9588.
[30] H.S. Liu, K. Ishida, Z.P. Jin, Y. Du, Intermetallics 11 (2003) 987.
[31] H. Iwasaki, M. Hirabayashi, K. Fujiwara, D. Watanabe, S. Ogawa, J. Phys. Soc. Jpn. 15 (1960) 1771.
[32] H. Iwasaki, J. Phys. Soc. Jpn. 17 (1962) 1620.
[33] H. Iwasaki, J. Phys. Soc. Jpn. 20 (1965) 2129.
[34] W.B. Pearson, J. Less-Common Met. 68 (1979) P9.
[35] H. Ipser, R. Krachler, Scr. Metall. 22 (1988) 1651.
[36] H. Okamoto, T.B. Massalski, Bull. Alloy Phase Diag. 10 (1989) 59.
[37] R. Prasad, M. Bienzie, F. Sommer, J. Alloys Compd. 200 (1993) 69.
[38] J.P. Jan, W.B. Pearson, Can. J. Phys. 42 (1964) 220.
[39] H. Pops, T.B. Massalski, Trans. AIME 233 (1965) 728.
[40] P.A. Goddard, J. Singleton, R.D. McDonald, N. Harrison, J.C. Lashley, H. Harima, M.-T. Suzuki, Phys. Rev. Lett. 94 (2005) 116401.
[41] K. Hisatsune, Y. Takuma, Y. Tanaka, K. Udoh, T. Morimura, M. Hasaka, Solid State Commun. 106 (1998) 509.
[42] J.H. Hodak, A. Henglein, M. Giersig, G.V. Hartland, J. Phys. Chem. B 104 (2000) 11708.
[43] M.P. Mallin, C.J. Murphy, Nano Lett. 2 (2002) 1235.
[44] R. Ferrando, J. Jellinek, R.L. Johnston, Chem. Rev. 108 (2008) 845.
[45] K.-S. Kim, J.-M. Yang, C.-H. Yu, I.-O. Jung, H.-H. Kim, J. Alloys Compd. 379 (2004) 314.
[46] R.L. Xu, Y.C. Lu, Y.J. Han, C. Wei, X. Wang, L.M. Yu, J. Mater. Sci.: Mater. Electr. 20 (2009) 675.
[47] W.-K. Liou, Y.-W. Yen, Intermetallics 17 (2009) 72.
[48] K. Krompholz, A. Weiss, J. Less-Common Met. 50 (1976) 213.
[49] A. Le Bail, H. Duroy, J.L. Fourquet, Mater. Res. Bull. 23 (1988) 447.
[50] V.-A. Edstrom, S. Westman, Acta Chem. Scand. 23 (1969) 279.
[51] H. Hiramatsu, F.E. Osterloh, Chem. Mater. 16 (2004) 2509.
[52] T. Pal, Mater. Manuf. Process 21 (2006) 315.
[53] X. Xiang, X.T. Zu, S. Zhu, C.F. Zhang, L.M. Wang, Nucl. Instrum. Methods Phys. Res., Sect. B 250 (2006) 192.
[54] H. Amekura, N. Umeda, K. Kono, Y. Takeda, N. Kishimoto, Ch. Buchal, S. Mantl, Nanotechnology 18 (2007) 395707.